Uniaxial Acoustic Vector Sensors for direction-of-arrival estimation

Ramamohan, Krishnaprasad Nambur; Comesaña, Daniel Fernandez; Leus, Geert

DOI
10.1016/j.jsv.2018.08.031

Publication date
2018

Document Version
Final published version

Published in
Journal of Sound and Vibration

Journal of Sound and Vibration 437 (2018) 276–291

Contents lists available at ScienceDirect

Journal of Sound and Vibration

journal homepage: www.elsevier.com/locate/jsvi

Uniaxial Acoustic Vector Sensors for direction-of-arrival estimation

Krishnaprasad Nambur Ramamohan [a,b,*], Daniel Fernandez Comesaña [a], Geert Leus [b]

[a] Microflown Technologies, 6824 BV Arnhem, The Netherlands
[b] Delft University of Technology, Mekelweg 2, 2628 CD Delft, The Netherlands

ARTICLE INFO

Article history:
Received 15 September 2017
Revised 23 July 2018
Accepted 15 August 2018
Available online 5 September 2018
Handling Editor: Y. Auregan

Keywords:
Acoustic Vector Sensor (AVS)
Direction-of-Arrival (DOA)
Array processing
Beampattern
Cramér-Rao Bound (CRB)
Mean Square Error (MSE)

ABSTRACT

In this paper, a specific reduced-channel Acoustic Vector Sensor (AVS) is proposed comprising one omni-directional microphone and only one particle velocity transducer, such that it can have an arbitrary orientation. Such a reduced transducer configuration is referred to as a Uniaxial AVS (U-AVS). The DOA performance of an array of U-AVSs is analyzed through its beampattern and compared to conventional configurations. It is shown that the U-AVS array beampattern results in an asymptotically biased estimate of the source location and it can be varied by choosing the orientation angles of the particle velocity transducers. Analytical expressions for the asymptotic bias of classical beamforming are proposed and verified both numerically as well as experimentally for Uniform Linear Arrays (ULAs). Furthermore, the Cramér-Rao Bound (CRB) and Mean Square Error (MSE) expressions are derived for a U-AVS array under a single source scenario and they are numerically evaluated for ULA. The implications of changing the orientations of the U-AVSs in the array on the MSE are discussed as well.

1. Introduction

Direction-of-Arrival (DOA) estimation of far-field acoustic sources is usually studied using a set of Acoustic Pressure Sensors (APSs) that are distributed spatially in an array configuration [1]. The interference pattern captured by the array of sensors provides acoustic information regarding the DOA of the far-field sources. The performance analysis of MUSIC (MUltiple SIgnal Classification) [2] and ML (Maximum Likelihood) [3] estimators, as well as the Cramér-Rao lower Bound (CRB) for an APS array have been thoroughly studied in the literature [4,5]. A comprehensive summary of existing techniques in the field of array signal processing can be found in Ref. [6]. On the other hand, with the advent of Micro-Electronic-Mechanical Systems (MEMS) technology it is nowadays feasible to manufacture acoustic probes that are capable of measuring particle velocity along with sound pressure, typically referred to as Acoustic Vector Sensors (AVSs) [7]. Each AVS typically comprises a pressure and three (two) particle velocity transducers in $\mathbb{R}^3(\mathbb{R}^2)$. The parameter estimation performance of an AVS array is proven to be better than that of the equivalent APS array as they make use of the interference pattern captured by the array of sensors as well as the intrinsic directionality of the sensors [8,9]. However, the number of data channels of an AVS measurement system is much larger compared to the traditional APS array, resulting in higher hardware complexity and power requirements. In this work,

* Corresponding author. Microflown Technologies, 6824 BV Arnhem, The Netherlands.
E-mail addresses: k.namburramamohan@tudelft.nl, ramamohan@microflown.com (K.N. Ramamohan), fernandez@microflown.com (D.F. Comesaña), g.j.t.leus@tudelft.nl (G. Leus).

https://doi.org/10.1016/j.jsv.2018.08.031
0022-460X/

we consider an alternative configuration of an AVS consisting of less particle velocity transducers, which preserves the benefits of conventional AVSs to a considerable extent.

A large and growing body of literature has developed the foundations of AVSs, including the sensor operation, manufacturing [7] and related array signal processing techniques. Unlike the APS, a single AVS can still be used for DOA estimation by exploiting its intrinsic directionality. In Ref. [10], the DOA estimation performance using an AVS is compared with various configurations of an APS array for a wide-band source. The maximum likelihood (ML) DOA estimator using an AVS is derived in Ref. [11]. Furthermore, the use of an AVS in source tracking applications has attracted lot of attention in the recent years [12–15]. As an extension, performance bounds on the DOA estimation error (CRB and angular mean square error) using AVS arrays were introduced in Ref. [9]. Over the following years, it was demonstrated that AVS arrays have distinct advantages over traditional pressure sensor arrays such as improved array gain and directional sensitivity [8,16]. In addition, it was demonstrated that an AVS array with a small and limited aperture significantly outperforms an APS array of the same length, as an AVS makes use of the full acoustic information available at its spatial location [8,9]. This aspect is key to maximize the performance achieved on space-limited platforms such as vehicles, unmanned aerial vehicles or smart glasses [17].

Conventional and MVDR (Minimum Variance Distortion-less Response) beamformers were initially extended to an AVS array in Refs. [8,16], showing that the DOA estimation performance improvements are more significant for smaller arrays, with simple structures, and in low SNR scenarios. Furthermore, it was shown in Refs. [18,19] that the beampattern of an AVS array can be expressed as a function of the conventional APS array, resulting in a combination of the information extracted from the spatial interference between the waveforms observed by the sensors and the intrinsic directivity of the particle velocity transducers. On the other hand, the role played by the array geometry on the performance of DOA estimation is considered in Ref. [20]. Based on the linear independence of the array manifold matrix, the maximum number of identifiable sources for under-sampled, over-sampled and critically-sampled AVS Uniform Linear Arrays (ULAs) is discussed in Ref. [21]. The extension of DOA estimation in the presence of coherent sources using AVS arrays was considered in Ref. [12]. Also in Refs. [22–24], the discussion of AVS arrays extends to environments with reflections and ambient noise.

For classical AVS, all the pressure and vector transducers coincide at the same spatial point, which is difficult to achieve in hardware. In practice, it is currently possible to integrate all the transducers required to construct an AVS within a sphere of 5 mm radius. As an alternative to the AVS, the use of non-collocated transducers comprised of a vector sensor has also been explored in the recent literature. In Refs. [25–27], the performance of DOA estimators of multiple spatially spread configurations were considered using a single pressure and up to three orthogonally oriented particle velocity transducers. It was shown that the Root Mean Square Error (RMSE) of the DOA estimates related to those configurations is better than that of one collocated AVS. Similar extensions of various configurations can be found in Refs. [28–30].

In this work, we look at a different implementation of an AVS comprising of only two transducers per sensor that are collocated, including one acoustic sound pressure and one particle velocity transducer with arbitrary orientation. Such a configuration is referred to as a Uniaxial AVS (U-AVS), as it captures only one component of the particle velocity field. The application of a U-AVS instead of an AVS removes one (for $\mathbb{R}^2$) or two (for $\mathbb{R}^3$) data channels per sensor, hence substantially lowering hardware and power requirements. The use of multiple U-AVSs can potentially be used for DOA estimation. However, the theoretical limits of such a configuration are not yet well understood. The motivation of this work is to explore how close the performance of a U-AVS array is in comparison with an equivalent aperture AVS array and conventional APS array. The main contributions of this work can be summarized as follows:

- A generalized framework is hereby introduced that accounts for any number of U-AVSs with arbitrary positions and orientations.
- We show that classical beamforming for a U-AVS array results in biased estimates of the DOA, due to which the Mean Square Error (MSE) bound, rather than the Cramér-Rao lower Bound (CRB), is considered as a theoretical criterion for assessing the performance of any DOA estimator and is compared with respect to the equivalent APS/AVS array.
- Both numerical and experimental results are provided in this work to validate the suggested expressions and show the feasibility of a practical implementation of the proposed array configuration.

For the sake of simplicity we restrict our discussion to $\mathbb{R}^2$ and focus on the estimation of the azimuth angle. However, the proposed model with a reduced number of particle velocity transducers (i.e., U-AVSs) can be extended to $\mathbb{R}^3$ for the estimation of both the azimuth and elevation angle. On the other hand, all the variants discussed in Refs. [25–30] can be considered as a specific case of the U-AVS array, with limited spatial locations. Those variants can be realized by considering either a pressure or a particle velocity transducer present at each spatial location.

The structure of the paper is as follows. In Section 2, we consider the measurement model of the multi-sensor multi-source AVS array. In Section 3, we describe the measurement model of the U-AVS array and subsequently the beampattern of the U-AVS array is analyzed. In Section 4, based on the first-order Taylor series expansion of the conventional beamforming function, we derive the bias in DOA estimation of a U-AVS array. In Section 5, we derive the biased CRB expression for a U-AVS array with a single far-field source in its field of view and further compare it with the CRB expressions of an equivalent aperture APS and AVS array. Finally, we suggest a MSE based design criterion upon which an optimal orientation for each of the U-AVSs in the array can be chosen. In Section 6, an experimental study is presented, including details about the measurement process. This study is used to verify the beampattern variations of a U-AVS array and also to validate the proposed analytical expressions that predict

the bias induced by the use of a U-AVS array.

The notation used in this paper can be described as follows: Upper (lower) bold face letters are used for matrices (column vectors); $(\cdot)^T$ denotes transpose and $(\cdot)^H$ denotes conjugate transpose; For any vectors $\mathbf{a}$ and $\mathbf{b}$, $(\mathbf{a}\cdot\mathbf{b})$ denotes the inner product between them. $\otimes$ denotes the Kronecker product and $\odot$ denotes the Schur-Hadamard (element-wise) product; $\mathbb{E}\{\cdot\}$ denotes the expectation operator; $\mathrm{tr}(\cdot)$ denotes the trace operator and $\mathbf{I}_n$ is an identity matrix of dimension n.

2. Review of beampattern analysis of AVS array

2.1. Measurement model of an AVS array

The measurement data of M AVSs and D far-field narrow-band sources present in a homogeneous isotropic medium at a discrete time index t of the measured snapshot corresponding to frequency f (wavelength λ) can be modeled as [9]:

$$\mathbf{y}(t) = \underbrace{\begin{bmatrix}\mathbf{a}(\phi_1) & \mathbf{a}(\phi_2) & \dots & \mathbf{a}(\phi_D)\end{bmatrix}}_{\mathbf{A}(\boldsymbol{\phi})} \underbrace{\begin{bmatrix} s_1(t) \\ s_2(t) \\ \cdot \\ \cdot \\ \cdot \\ s_D(t)\end{bmatrix}}_{\mathbf{s}(t)} + \mathbf{n}(t) \in \mathbb{C}^{3M\times 1}, \tag{1}$$

where $\boldsymbol{\phi} = \begin{bmatrix}\phi_1 & \phi_2 & \dots & \phi_D\end{bmatrix}^T \in \mathbb{R}^{D\times 1}$ collects the azimuth angles of all the D far-field sources, $\mathbf{s}(t)$ is the source signal vector, $\mathbf{n}(t)$ is the additive noise vector present in the measurement data, and $\mathbf{a}(\phi_d)$ is the AVS array manifold vector of the dth source which can be expressed as $\mathbf{a}(\phi_d) = \mathbf{a}_\mathrm{p}(\phi_d)\otimes\mathbf{h}(\phi_d)$. Here $\mathbf{a}_\mathrm{p}(\phi_d)$ denotes the equivalent APS array manifold vector and $\mathbf{h}(\phi_d)$ denotes the directional information obtained through the vector sensors,

$$\begin{aligned}\mathbf{a}_\mathrm{p}(\phi_d) &= \begin{bmatrix} e^{\mathrm{j}k(\mathbf{r}_1\cdot\mathbf{u}_d)} & e^{\mathrm{j}k(\mathbf{r}_2\cdot\mathbf{u}_d)} & \dots & e^{\mathrm{j}k(\mathbf{r}_M\cdot\mathbf{u}_d)}\end{bmatrix}^T \in \mathbb{C}^{M\times 1},\\ \mathbf{h}(\phi_d) &= \begin{bmatrix}1 & \mathbf{u}_d^T\end{bmatrix}^T \in \mathbb{R}^{3\times 1},\end{aligned} \tag{2}$$

where $k = \frac{2\pi}{\lambda} = \frac{2\pi f}{c}$ is the wave number of the narrow-band source signals, $\mathbf{r}_m$ represents the position of the mth AVS in the array, and $\mathbf{u}_d = \begin{bmatrix}\cos(\phi_d) & \sin(\phi_d)\end{bmatrix}^T$ is the unitary vector in the direction of the dth source. In the further discussion, it is assumed that the source and noise signals are a realization of an independent and identically distributed (i.i.d.), zero mean complex Gaussian process. The covariance matrix of $\mathbf{s}(t)$ is assumed to be $\mathbf{R}_\mathrm{s} = \mathbb{E}\left\{\mathbf{s}(t)\mathbf{s}^H(t)\right\} \in \mathbb{C}^{D\times D}$. The noise covariance matrix is modeled as $\mathbf{R}_\mathrm{n} = \mathbb{E}\left\{\mathbf{n}(t)\mathbf{n}^H(t)\right\} = \sigma_\mathrm{n}^2\boldsymbol{\Sigma} \in \mathbb{C}^{3\mathrm{M}\times 3\mathrm{M}}$, where $\boldsymbol{\Sigma}$ is a known positive definite Hermitian matrix. For a single AVS, $\boldsymbol{\Sigma}$ is given as:

$$\boldsymbol{\Sigma} = \begin{bmatrix}1 & \mathbf{0}^T \\ \mathbf{0} & \beta\,\mathbf{I}_2\end{bmatrix} \in \mathbb{C}^{3\times 3}, \tag{3}$$

where β is a gain term, that models the noise difference between the pressure and velocity channels. For the sake of simplicity, we consider $\boldsymbol{\Sigma} = \mathbf{I}_{3M}$ (or $\beta = 1$ for a single sensor). In practice, $\boldsymbol{\Sigma}$ can be estimated by assessing the noise floor of the sensors in the array. The effect of $\boldsymbol{\Sigma}$ (or β for a single sensor) is studied in Refs. [8,18,20,23].

2.2. Beampattern of an AVS array

Based on the measurement data model of the AVS array, the beampattern for a single source at DOA ϕ can be expressed as:

$$B(\widehat{\phi}) = |\mathbf{w}^H(\widehat{\phi})\,\mathbf{a}(\phi)|,\ -\pi < \widehat{\phi} \le \pi \tag{4}$$

where $\mathbf{w}(\widehat{\phi})$ is the weighting function, which is explicitly shown to be dependent on the scanning angle $\widehat{\phi}$. The choice of $\mathbf{w}(\widehat{\phi}) = \mathbf{a}(\widehat{\phi})$ results in the spatial response of the matched filter, leading to

$$\begin{aligned}B(\widehat{\phi},\phi) &= |\mathbf{a}^H(\widehat{\phi})\mathbf{a}(\phi)|,\\ &= \left|\left(\mathbf{h}^H(\widehat{\phi})\mathbf{h}(\phi)\right)\left(\mathbf{a}_\mathrm{p}^H(\widehat{\phi})\mathbf{a}_\mathrm{p}(\phi)\right)\right|,\end{aligned}$$

$$= \underbrace{\left(1 + \cos(\hat{\phi})\cos(\phi) + \sin(\hat{\phi})\sin(\phi)\right)}_{\mathrm{VGM}(\hat{\phi},\phi)} \underbrace{\left|\left(e^{\mathrm{j}k\left(\mathbf{r}_1\cdot\mathbf{u}(\phi)-\mathbf{r}_1\cdot\mathbf{u}(\hat{\phi})\right)} + \ldots + e^{\mathrm{j}k\left(\mathbf{r}_M\cdot\mathbf{u}(\phi)-\mathbf{r}_M\cdot\mathbf{u}(\hat{\phi})\right)}\right)\right|}_{B_{\mathrm{p}}(k,\hat{\phi},\phi)}. \tag{5}$$

The expression in Eq. (5) is similar to the expressions derived in Ref. [18] and it can be further simplified if the sensors of the array are arranged in a Uniform Linear Array (ULA) configuration along the x-axis with inter-sensor spacing d. Then the $B_{\mathrm{p}}(k,\hat{\phi},\phi)$ term in beampattern expression Eq. (5) can be modified as:

$$B_{\mathrm{p}}(k,\hat{\phi},\phi) = \underbrace{M\left|\frac{\mathrm{sinc}\left(\frac{kd}{2}M\left(\cos(\phi)-\cos(\hat{\phi})\right)\right)}{\mathrm{sinc}\left(\frac{kd}{2}\left(\cos(\phi)-\cos(\hat{\phi})\right)\right)}\right|}_{\text{APS ULA beampattern}}. \tag{6}$$

Here, the beampattern expression is described explicitly as a function of k, $\hat{\phi}$ and ϕ for the sake of analyzing beampatterns with changes in those parameters. It is interesting to note that the beampattern of an AVS ULA $B(k,\hat{\phi},\phi)$ is expressed as a product of the equivalent APS ULA beampattern $B_{\mathrm{p}}(k,\hat{\phi},\phi)$ and a Velocity Gain Modulation (VGM) term $\mathrm{VGM}(\hat{\phi},\phi)$. It should be noted that the $\mathrm{VGM}(\hat{\phi},\phi)$ term is independent of the number of sensors M and the wave number k of the source signal. Furthermore, Eq. (6) can also be expressed in terms of the frequency of the source signal by substituting $k\cdot d = \frac{\pi f}{f_d}$, where $f_d = \frac{c}{2d}$ is the design frequency of the array. The presence of the VGM term significantly attenuates the side lobes, suppresses left/right ambiguity and renders its applicability for DOA estimation under changes of the source signal frequency. An extended discussion on the beampattern of an AVS array can be found in Ref. [31].

3. Beampattern analysis of U-AVS array

3.1. Measurement model of a U-AVS array

We shall now consider a U-AVS based array with M sensors located at arbitrary positions indicated by the position vectors $\mathbf{r}_1, \mathbf{r}_2, \ldots, \mathbf{r}_M$ and D far-field sound sources located in the direction pointed by the unit vectors $\mathbf{u}_1, \mathbf{u}_2, \ldots, \mathbf{u}_D$. Each of the U-AVSs consists of a pressure sensor and a single particle velocity transducer, whose orientation is arbitrary and indicated by δ_n. The measurement data $\mathbf{y}(t)$ at a time index t of the measured snapshot corresponding to frequency f (wavelength λ) can be modeled as:

$$\mathbf{y}(t) = \underbrace{\left[\mathbf{a}(\phi_1,\boldsymbol{\delta}) \quad \mathbf{a}(\phi_2,\boldsymbol{\delta}) \quad \ldots \quad \mathbf{a}(\phi_D,\boldsymbol{\delta})\right]}_{\mathbf{A}(\boldsymbol{\phi},\boldsymbol{\delta})\in\mathbb{C}^{2M\times D}} \mathbf{s}(t) + \mathbf{n}(t) \in \mathbb{C}^{2M\times 1}, \tag{7}$$

where $\mathbf{a}(\phi_i,\boldsymbol{\delta}) = \left[e^{\mathrm{j}k(\mathbf{r}_1\cdot\mathbf{u}_i)} \quad e^{\mathrm{j}k(\mathbf{r}_1\cdot\mathbf{u}_i)}\cos(\delta_1-\phi_i) \quad \ldots \quad e^{\mathrm{j}k(\mathbf{r}_M\cdot\mathbf{u}_i)} \quad e^{\mathrm{j}k(\mathbf{r}_M\cdot\mathbf{u}_i)}\cos(\delta_M-\phi_i)\right]^T$ is the array response vector of the ith source with each U-AVS having an arbitrary orientation captured by the vector $\boldsymbol{\delta} = \left[\delta_1 \quad \delta_2 \quad \ldots \quad \delta_M\right]^T$, $\mathbf{s}(t)$ is the source signal vector and $\mathbf{n}(t)$ is the additive noise vector present in the measurement data. In the further discussion, we refer this setup as a U-AVS array with an arbitrary orientation or just a U-AVS array. If all the U-AVSs have the same orientation angle, i.e., $\boldsymbol{\delta} = \delta\left[1 \quad 1 \quad \ldots \quad 1\right]^T$, which is a specific case of a U-AVS array with an arbitrary orientation, we refer to it as a U-AVS array with fixed orientation.

3.2. Beampattern of a U-AVS array

Based on the matched filter approach for given sensor orientation angles $\boldsymbol{\delta}$, the beampattern expression from Eq. (5) for a single source at DOA ϕ is modified as:

$$\begin{aligned} B(\hat{\phi},\phi) &= \left|\mathbf{a}^H(\hat{\phi},\boldsymbol{\delta})\,\mathbf{a}(\phi,\boldsymbol{\delta})\right|, \\ &= \left|\left(1+\cos(\delta_1-\hat{\phi})\cos(\delta_1-\phi)\right)e^{\mathrm{j}k\left(\mathbf{r}_1\cdot\mathbf{u}(\phi)-\mathbf{r}_1\cdot\mathbf{u}(\hat{\phi})\right)} + \ldots + \left(1+\cos(\delta_M-\hat{\phi})\cos(\delta_M-\phi)\right)e^{\mathrm{j}k\left(\mathbf{r}_M\cdot\mathbf{u}(\phi)-\mathbf{r}_M\cdot\mathbf{u}(\hat{\phi})\right)}\right|, \end{aligned} \tag{8}$$

and for a U-AVS array with fixed orientation (δ), the beampattern expression can be simplified as:

$$B(k,\hat{\phi},\phi) = \mathrm{VGM}(\delta,\hat{\phi},\phi)\,B_{\mathrm{p}}(k,\hat{\phi},\phi), \tag{9}$$

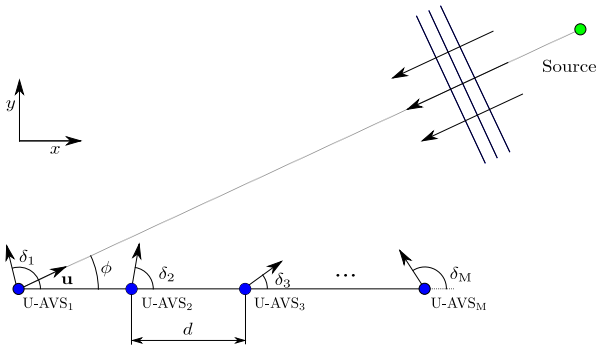

Fig. 1. ULA of M U-AVSs and one source. Each U-AVS is represented by a combination of a dot corresponding to an APS and a black arrow corresponding to a particle velocity transducer where δ_n represents the orientation of the nth U-AVS.

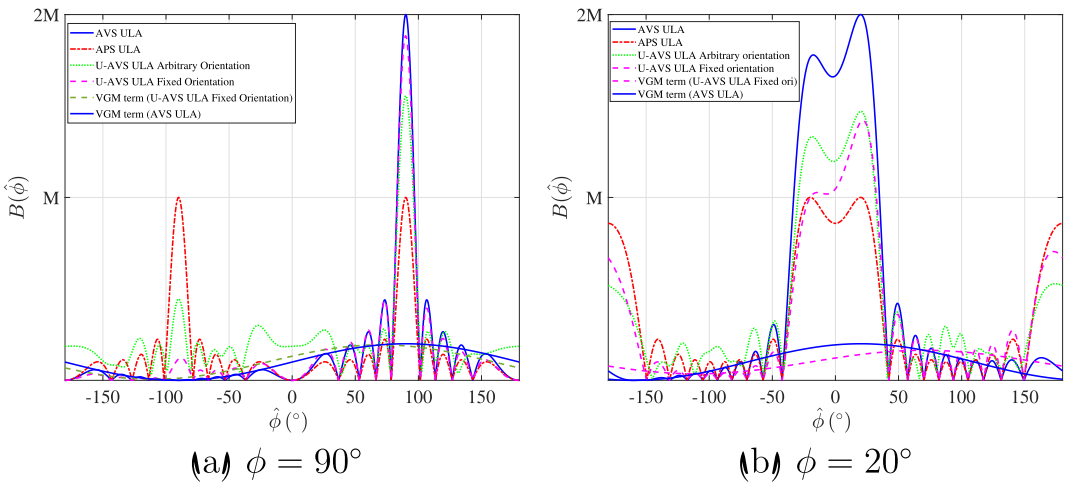

Fig. 2. Beampattern of an AVS, APS and U-AVS ULA with a fixed and arbitrary orientation for $M = 10, f = f_d$. For the U-AVS ULA with fixed orientation, $\delta = 70°$, and for a U-AVS ULA with arbitrary orientation, $\boldsymbol{\delta} = [10°, 118°, 75°, 49°, 138°, 85°, 107°, 25°, 144°, 37°]$.

where

$$\mathrm{VGM}(\delta, \hat{\phi}, \phi) = 1 + \cos(\delta - \hat{\phi})\cos(\delta - \phi). \tag{10}$$

It can again be observed that Eq. (9) can be expressed as the product of an equivalent APS array beampattern and the VGM term.

Restricting our study to a ULA as depicted in Fig. 1, and expressing the beampattern explicitly as a function of k, $\hat{\phi}$, ϕ by substituting $\mathbf{a}(\hat{\phi}, \boldsymbol{\delta})$ of Eq. (7) into Eq. (8) results in:

$$\begin{aligned} B(k, \hat{\phi}, \phi) = | &\left(1 + \cos(\delta_1 - \hat{\phi})\cos(\delta_1 - \phi)\right) + e^{\mathrm{j}kd(\cos(\phi) - \cos(\hat{\phi}))}\left(1 + \cos(\delta_2 - \hat{\phi})\cos(\delta_2 - \phi)\right) + \ldots \\ &+ e^{\mathrm{j}k(M-1)d(\cos(\phi) - \cos(\hat{\phi}))}\left(1 + \cos(\delta_M - \hat{\phi})\cos(\delta_M - \phi)\right) | \,. \end{aligned} \tag{11}$$

For a fixed orientation scenario this leads to $B(k, \hat{\phi}, \phi) = \mathrm{VGM}(\delta, \hat{\phi}, \phi)\, B_{\mathrm{p}}(k, \hat{\phi}, \phi)$ with $\mathrm{VGM}(\delta, \hat{\phi}, \phi)$ as in Eq. (10) and $B_p(k, \hat{\phi}, \phi)$ as in Eq. (6). In Fig. 2, the beampatterns of an AVS, APS, U-AVS ULA with a fixed and arbitrary orientation for a single source are plotted. The orientation angle, δ, for a fixed orientation configuration is chosen to be 70° and for an arbitrary orientation configuration it is chosen randomly between 0° and 180°. The VGM terms of an AVS ULA and U-AVS ULA with a fixed orientation are also plotted in Fig. 2.

By observing closely the VGM term of the U-AVS ULA with a fixed orientation in Eq. (10) and Fig. 2, the maximum will always occur at $\hat{\phi} = \delta$, irrespective of the actual DOA ϕ. As the APS ULA beampattern always provides an unbiased source location estimate, a bias will be introduced by the VGM term. As the aperture of the ULA increases (i.e., as the number of sensors increases with a fixed inter-sensor spacing d), the main lobe of the APS ULA beampattern becomes narrower whereas the $\mathrm{VGM}(\delta, \hat{\phi}, \phi)$ term is unaffected. Hence, the bias is expected to decrease as the aperture increases. On the other hand, for a fixed aperture, the bias can be controlled by changing the orientation angle(s) of the U-AVSs. Hence the rate of decrease of the bias depends on the

aperture of the array, sensor orientation angles $\boldsymbol{\delta}$ and the DOA. In Section 4 we shall quantify the behavior of the bias in the DOA estimates of a U-AVS ULA.

4. Bias analysis of a U-AVS array

The DOA estimates based on the spatial response of different beamformers (classical and Capon) or based on MUSIC, are all obtained by maximizing or minimizing the following generalized expression:

$$f(\phi) = \mathbf{a}^H(\phi)\,\mathbf{R}\,\mathbf{a}(\phi), \tag{12}$$

where for classical beamforming $\mathbf{R}$ is the covariance matrix ($\mathbf{R_y}$) of the measurement data ($\mathbf{y}$), for Capon beamforming $\mathbf{R}$ is the inverse of the covariance matrix ($\mathbf{R_y^{-1}}$), and for MUSIC $\mathbf{R}$ is the outer product of the unitary matrix which spans the null subspace of the covariance matrix ($\mathbf{R_y}$). The estimates of ϕ (here denoted as ϕ_e) are the maximizers or minimizers of $f(\phi)$. They can be obtained by setting $\frac{\partial f(\phi)}{\partial \phi}|_{\phi=\phi_e} = \frac{\partial f(\phi_e)}{\partial \phi}$ to zero. By using a Taylor series expansion of $\frac{\partial f(\phi_e)}{\partial \phi}$ around the true ϕ and by considering the first two terms in it, we can approximate $\frac{\partial f(\phi_e)}{\partial \phi}$ as in Ref. [8]:

$$\begin{aligned} &\frac{\partial f(\phi_e)}{\partial \phi} \approx \frac{\partial f(\phi)}{\partial \phi} + \frac{\partial^2 f(\phi)}{\partial \phi^2}(\phi_e - \phi) = 0, \\ &\implies b(\phi) = \underbrace{(\phi_e - \phi)}_{\text{bias}} \approx \widehat{b}(\phi) = -\left[\frac{\partial^2 f(\phi)}{\partial \phi^2}\right]^{-1} \frac{\partial f(\phi)}{\partial \phi}. \end{aligned} \tag{13}$$

From Eq. (13) it can be seen that the bias in the estimate of the source location is approximated based on the first and second derivatives of the spatial spectrum function $f(\cdot)$ evaluated at ϕ. For a U-AVS array and considering the classical beamforming approach, an analytical expression for the bias based on Eq. (13), where $f(\phi) = \mathbf{a}^H(\phi)\mathbf{R_y}\mathbf{a}(\phi)$ and $\mathbf{R_y} = \sigma_s^2\mathbf{a}(\boldsymbol{\delta},\phi)\mathbf{a}^H(\boldsymbol{\delta},\phi) + \sigma_n^2\mathbf{I}$, is given by (derived in Appendix A):

$$\widehat{b}(\phi) = -\frac{\mathrm{SNR}\,(RS) + S}{\mathrm{SNR}\left(RJ + L^2 + S^2\right) + J + W}, \tag{14}$$

where,

$$\mathrm{SNR} = \frac{\text{Source power}}{\text{Noise power}} = \frac{\sigma_s^2}{\sigma_n^2},$$

$$R = M + \sum_{i=1}^{M} \cos^2(\delta_i - \phi),$$

$$S = \sum_{i=1}^{M} \cos(\delta_i - \phi)\sin(\delta_i - \phi),$$

$$J = -k^2 \sum_{i=1}^{M} \left(\mathbf{r}_i \cdot \frac{\partial \mathbf{u}}{\partial \phi}\right)^2 \left(1 + \cos^2(\delta_i - \phi)\right) - \sum_{i=1}^{M} \cos^2(\delta_i - \phi),$$

$$L = k \sum_{i=1}^{M} \left(\mathbf{r}_i \cdot \frac{\partial \mathbf{u}}{\partial \phi}\right) \left(1 + \cos^2(\delta_i - \phi)\right),$$

$$W = k^2 \sum_{i=1}^{M} \left(\mathbf{r}_i \cdot \frac{\partial \mathbf{u}}{\partial \phi}\right)^2 \left(1 + \cos^2(\delta_i - \phi)\right) + \sum_{i=1}^{M} \sin^2(\delta_i - \phi).$$

If value of SNR tends to 0, the expression for the bias in Eq. (14) reduces to:

$$\widehat{b}_0(\phi) = -\frac{S}{J + W}. \tag{15}$$

Asymptotically (i.e., as SNR $\to \infty$), the expression for the bias in Eq. (14) reduces to:

$$\widehat{b}_\infty(\phi) = -\frac{RS}{RJ + L^2 + S^2}. \tag{16}$$

In practice, the bias ($\widehat{b}(\phi)$) in the DOA estimate lies between $\widehat{b}_0(\phi)$ and $\widehat{b}_\infty(\phi)$ (i.e., $\widehat{b}_0(\phi) < \widehat{b}(\phi) < \widehat{b}_\infty(\phi)$) for $0 < \mathrm{SNR} < \infty$. It is to be noted that the J and L terms in Eq. (16) will have a more dominant contribution to the bias expression as the number

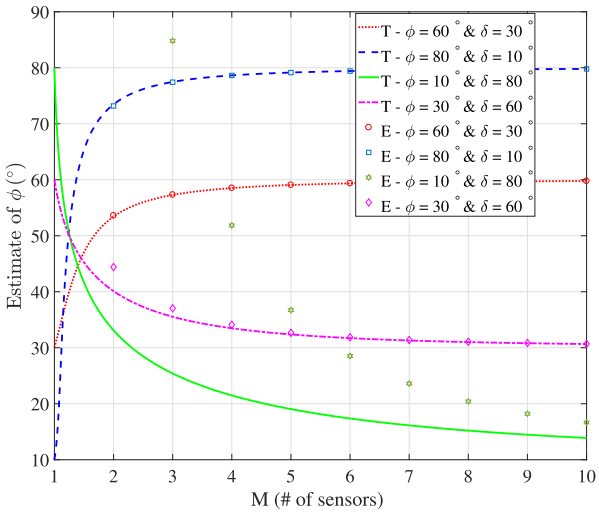

Fig. 3. Comparison of the source DOA estimates based on a U-AVS ULA with a fixed orientation beampattern (continuous lines, labeled 'T') and based on the asymptotic bias expression Eq. (16) (discrete markers, labeled 'E') for different DOAs and sensor orientations with an increasing aperture of the ULA.

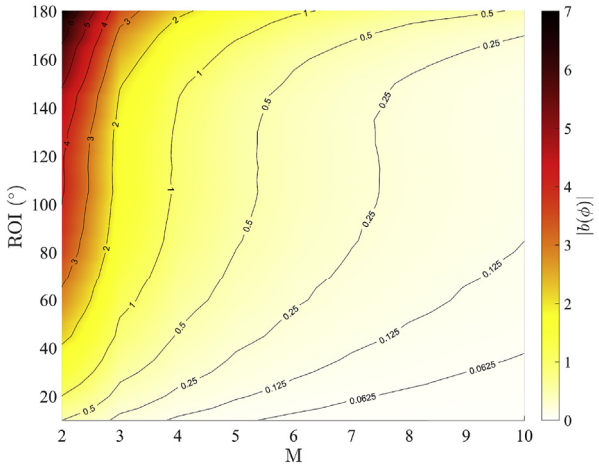

Fig. 4. Monte Carlo simulation results to study the average bias of the U-AVS ULA with multiple sensors and considering a variable ROI.

of elements in the array/aperture of the array increases. Based on Eq. (16) and by considering a U-AVS ULA with a fixed orientation (δ), the derived bias of the source location $\left(\widehat{b}(\phi)\right)$ is compared to the bias of the actual estimate ($b(\phi)$) obtained by the beampattern expression Eq. (9) in Fig. 3. As seen in Fig. 3, the first order approximation becomes worse if the angle of arrival is closer to the end-fire direction and the sensor orientation is near the broadside region (as seen for $\phi = 10^\circ$ and $\delta = 80^\circ$). It can also be observed that as the number of sensors (or aperture) increases, the approximation of the bias expression improves and the rate of improvement depends on the sensor orientation angle δ and the DOA.

Furthermore, a Monte Carlo simulation for a single source scenario is performed to understand the average bias of a U-AVS ULA. The simulation considers multiple sensors oriented within a variable angular region-of-interest (ROI) centered around the broadside of the array. For a given number of sensors and ROI, 5000 iterations were performed. Within each iteration, both the DOA and the orientations of the sensors are derived from a realization of a uniform distribution within the ROI. The results are presented in Fig. 4, where the bias is obtained based on the beampattern expression Eq. (9). A large bias is only observed for configurations with a few sensors and a wide angular ROI. As the number of sensors increases, the bias becomes negligible.

5. Review of Cramér-Rao bounds for AVS, U-AVS and APS array

To analyze the minimum attainable error covariance matrix of a DOA estimator, we have evaluated the Cramér-Rao lower Bound (CRB) for multiple sensor configurations with a single source in its field-of-view.

5.1. CRB for multi-sensor and multi-source configuration

The generalized sensor array data model can be written as:

$$\mathbf{y}(t) = \mathbf{A}(\boldsymbol{\phi})\,\mathbf{s}(t) + \mathbf{n}(t), \tag{17}$$

where $\boldsymbol{\phi} = \begin{bmatrix}\phi_1 & \phi_2 & \dots & \phi_D\end{bmatrix}^T \in \mathbb{R}^{D\times 1}$.

Note that Eq. (17) is same as:

- Eq. (1) for an AVS array;
- Eq. (7) for a U-AVS array, except that the dependency on the sensor orientation angles $\boldsymbol{\delta}$ is dropped;
- Eq. (1) for an APS array, if $\mathbf{h}(\phi_n) = \begin{bmatrix}1\end{bmatrix}, \forall n = 1, \dots, D$.

It is assumed that the source signals $\mathbf{s}(t)$ and the noise $\mathbf{n}(t)$ are realizations of an i.i.d. complex Gaussian process with zero mean and unknown covariance $\mathbf{R_s}$ and $\mathbf{R_n} = \sigma_n^2\mathbf{I}$. The CRB on the error covariance matrix of any (locally) unbiased estimator of the vector $\boldsymbol{\phi}$ of the physical process described in Eq. (17) is given by Refs. [9,32]:

$$\mathrm{CRB}(\boldsymbol{\phi}) = \mathbf{J}^{-1}(\boldsymbol{\phi}) = \frac{\sigma_n^2}{2N}\left(\mathrm{Re}\left[\mathbf{U}\odot\left(\mathbf{D}^H\boldsymbol{\Pi}_c\mathbf{D}\right)^T\right]\right)^{-1}, \tag{18}$$

where $\mathbf{U} = \mathbf{R_s}\left(\mathbf{A}^H\mathbf{A}\mathbf{R_s} + \sigma_n^2\mathbf{I}\right)^{-1}\mathbf{A}^H\mathbf{A}\,\mathbf{R_s}$, $\boldsymbol{\Pi}_c = \mathbf{I} - \boldsymbol{\Pi}$, $\boldsymbol{\Pi} = \mathbf{A}\left(\mathbf{A}^H\mathbf{A}\right)^{-1}\mathbf{A}^H$, $\mathbf{D} = \begin{bmatrix}\mathbf{d}(\phi_1) & \dots & \mathbf{d}(\phi_D)\end{bmatrix}$, $\mathbf{d}(\phi_n) = \frac{\partial\mathbf{a}(\phi_n)}{\partial\phi_n}$, $\forall n = 1, \dots, D$, $\mathrm{Re}[\cdot]$ represents the real part of the argument, $\mathbf{J}(\boldsymbol{\phi})$ is the Fisher-information matrix, and N is the number of time snapshots considered for evaluating the CRB.

As we have seen, a U-AVS array introduces a bias in the estimate when it is used in combination with the classical beamforming approach, which becomes more apparent when the aperture is small. The CRB for biased estimators can be obtained by a simple modification of Eq. (18). Let $\widehat{\boldsymbol{\phi}}$ denote an arbitrary estimator of $\boldsymbol{\phi}$ with bias $\mathbf{b}(\boldsymbol{\phi})$. Then the CRB for such a biased estimator is given by Ref. [33]:

$$\mathrm{CRB_b}(\boldsymbol{\phi}) = \left(\mathbf{I} + \mathbf{D}(\boldsymbol{\phi})\right)\mathbf{J}^{-1}(\boldsymbol{\phi})\left(\mathbf{I} + \mathbf{D}(\boldsymbol{\phi})\right)^T, \tag{19}$$

where $\mathbf{J}^{-1}(\boldsymbol{\phi})$ is the inverse of the Fisher information matrix as seen in Eq. (18) and $\mathbf{D}(\boldsymbol{\phi})$ is the bias gradient matrix defined by:

$$\mathbf{D}(\boldsymbol{\phi}) = \frac{\partial\mathbf{b}(\boldsymbol{\phi})}{\partial\boldsymbol{\phi}}. \tag{20}$$

It can be seen that the CRB of a biased estimator depends on the bias variations rather than the bias itself. Also in the case of a biased estimator, the Mean Square Error (MSE) is a direct measure of the estimator's performance and it can be written as:

$$\mathrm{MSE}(\boldsymbol{\phi}) = \mathbb{E}\left\{\left\|\widehat{\boldsymbol{\phi}} - \boldsymbol{\phi}\right\|^2\right\} = \left\|\mathbf{b}(\boldsymbol{\phi})\right\|^2 + \mathrm{tr}\left(\mathrm{CRB_b}(\boldsymbol{\phi})\right). \tag{21}$$

5.2. Evaluation of CRB for a single source

This section is focused on evaluating the CRB of an AVS, U-AVS and APS array with a single far-field source in its field of view. For the given scenario with $\mathbb{E}\left\{s(t)s^H(t)\right\} = \sigma_s^2$, Eq. (18) yields:

$$\mathrm{CRB}(\phi) = \frac{\sigma_n^2}{2N}\frac{1}{\mathrm{Re}\left[U\left(\mathbf{d}^H(\phi)\boldsymbol{\Pi}_c\mathbf{d}(\phi)\right)\right]}, \tag{22}$$

where $U = \frac{\left(\mathbf{a}^H(\phi)\mathbf{a}(\phi)\right)\sigma_s^4}{\left(\mathbf{a}^H(\phi)\mathbf{a}(\phi)\right)\sigma_s^2+\sigma_n^2}$, $\mathbf{d}(\phi) = \frac{\partial\mathbf{a}(\phi)}{\partial\phi}$ and $\boldsymbol{\Pi} = \frac{\mathbf{a}(\phi)\mathbf{a}^H(\phi)}{\mathbf{a}^H(\phi)\mathbf{a}(\phi)}$.

Based on Eq. (22), assuming a locally unbiased estimator, the expressions of the CRB for various scenarios are derived in Appendix B. Using $\mathrm{SNR} = \frac{\sigma_s^2}{\sigma_n^2}$, the expressions of this CRB for various sensor configurations are presented in Table 1, where

$$\begin{aligned} P_G = {} & Mk^2\sum_{i=1}^{M}\left(\mathbf{r}_i\cdot\frac{\partial\mathbf{u}}{\partial\phi}\right)^2\left(1+\cos^2(\delta_i-\phi)\right) + M\sum_{i=1}^{M}\sin^2(\delta_i-\phi) - k^2\sum_{i=1}^{M}\sum_{j=1}^{M}\left(\mathbf{r}_i\cdot\frac{\partial\mathbf{u}}{\partial\phi}\right)\left(\mathbf{r}_j\cdot\frac{\partial\mathbf{u}}{\partial\phi}\right) \\ & \left(1+\cos^2(\delta_i-\phi)\right) + k^2\sum_{i=1}^{M}\sum_{j=1}^{M}\left(\left(\mathbf{r}_i\cdot\frac{\partial\mathbf{u}}{\partial\phi}\right)^2 - \left(\mathbf{r}_i\cdot\frac{\partial\mathbf{u}}{\partial\phi}\right)\left(\mathbf{r}_j\cdot\frac{\partial\mathbf{u}}{\partial\phi}\right)\right)\cos^2(\delta_j-\phi)\left(1+\cos^2(\delta_i-\phi)\right) \\ & + \sum_{i=1}^{M}\sum_{j=1}^{M}\left(\cos^2(\delta_j-\phi)\sin^2(\delta_i-\phi) - \cos(\delta_i-\phi)\,\sin(\delta_i-\phi)\,\cos(\delta_j-\phi)\,\sin(\delta_j-\phi)\right). \end{aligned} \tag{23}$$

Table 1
CRB for several sensor array configurations.

	CRB
APS	$\frac{1}{2N\left(Mk^2\sum_{i=1}^{M}\left(\mathbf{r}_i\cdot\frac{\partial\mathbf{u}}{\partial\phi}\right)^2-k^2\sum_{i=1}^{M}\sum_{j=1}^{M}\left(\mathbf{r}_i\cdot\frac{\partial\mathbf{u}}{\partial\phi}\right)\left(\mathbf{r}_j\cdot\frac{\partial\mathbf{u}}{\partial\phi}\right)\right)}\left(\frac{M}{\mathrm{SNR}}+\frac{1}{(\mathrm{SNR})^2}\right)$
AVS	$\frac{1}{2N\left(4Mk^2\sum_{i=1}^{M}\left(\mathbf{r}_i\cdot\frac{\partial\mathbf{u}}{\partial\phi}\right)^2+2M^2-4k^2\sum_{i=1}^{M}\sum_{j=1}^{M}\left(\mathbf{r}_i\cdot\frac{\partial\mathbf{u}}{\partial\phi}\right)\left(\mathbf{r}_j\cdot\frac{\partial\mathbf{u}}{\partial\phi}\right)\right)}\left(\frac{2M}{\mathrm{SNR}}+\frac{1}{(\mathrm{SNR})^2}\right)$
U-AVS	$\frac{1}{2NP_G}\left(\frac{\left(M+\sum_{i=1}^{M}\cos^2(\delta_i-\phi)\right)}{\mathrm{SNR}}+\frac{1}{(\mathrm{SNR})^2}\right)$

For the particular case of a U-AVS ULA with a fixed orientation, $\delta_i = \delta, \forall i = 1, 2, \ldots, M$, the expression of the CRB can be simplified yielding:

$$\mathrm{CRB}(\phi) = \frac{1}{2NP_G}\left(\frac{M\left(1+\cos^2(\delta-\phi)\right)}{\mathrm{SNR}}+\frac{1}{(\mathrm{SNR})^2}\right), \tag{24}$$

where

$$P_G = Mk^2\left(1+\cos^2(\delta-\phi)\right)\sum_{i=1}^{M}\left(\mathbf{r}_i\cdot\frac{\partial\mathbf{u}}{\partial\phi}\right)^2 + M^2\sin^2(\delta-\phi) - k^2\left(1+\cos^2(\delta-\phi)\right)\sum_{i=1}^{M}\sum_{j=1}^{M}\left(\mathbf{r}_i\cdot\frac{\partial\mathbf{u}}{\partial\phi}\right)\left(\mathbf{r}_j\cdot\frac{\partial\mathbf{u}}{\partial\phi}\right)$$
$$+ k^2\cos^2(\delta-\phi)\left(1+\cos^2(\delta-\phi)\right)\sum_{i=1}^{M}\sum_{j=1}^{M}\left(\left(\mathbf{r}_i\cdot\frac{\partial\mathbf{u}}{\partial\phi}\right)^2-\left(\mathbf{r}_i\cdot\frac{\partial\mathbf{u}}{\partial\phi}\right)\left(\mathbf{r}_j\cdot\frac{\partial\mathbf{u}}{\partial\phi}\right)\right). \tag{25}$$

As we have seen, the conventional DOA estimate based on the beampattern for a U-AVS array results in a biased estimate. The bias in the DOA estimate for a U-AVS array is quantified in Eq. (14). We can thus also consider the modified CRB expression of Eq. (19) for biased estimates ($\mathrm{CRB_b}$), which incorporates the rate of change in the bias term:

$$\mathrm{CRB_b}(\phi) = \left(1+\frac{\partial b(\phi)}{\partial\phi}\right)^2\mathrm{CRB}(\phi), \quad \approx \left(1+\frac{\partial\widehat{b}(\phi)}{\partial\phi}\right)^2\mathrm{CRB}(\phi), \tag{26}$$

where

$$\frac{\partial\widehat{b}(\phi)}{\partial\phi} = -\frac{1}{Q^2}\left[Q\left(\mathrm{SNR}\left(R\frac{\partial S}{\partial\phi}+\frac{\partial R}{\partial\phi}S\right)+\frac{\partial S}{\partial\phi}\right)-\mathrm{SNR}\left(\mathrm{SNR}\left(RS\right)+S\right)\left(\frac{\partial R}{\partial\phi}J+R\frac{\partial J}{\partial\phi}+2S\frac{\partial S}{\partial\phi}+2L\frac{\partial L}{\partial\phi}\right)\right], \tag{27}$$

$$Q = \mathrm{SNR}\left(RJ+S^2+L^2\right)+J+W, \tag{28}$$

$$\frac{\partial R}{\partial\phi} = 2\sum_{i=1}^{M}\cos(\delta_i-\phi)\sin(\delta_i-\phi), \tag{29}$$

$$\frac{\partial S}{\partial\phi} = \sum_{i=1}^{M}\left(\sin^2(\delta_i-\phi)-\cos^2(\delta_i-\phi)\right), \tag{30}$$

$$\frac{\partial L}{\partial\phi} = k\sum_{i=1}^{M}\left[\left(\mathbf{r}_i\cdot\frac{\partial^2\mathbf{u}}{\partial\phi^2}\right)\left(1+\cos^2(\delta_i-\phi)\right)+\left(\mathbf{r}_i\cdot\frac{\partial\mathbf{u}}{\partial\phi}\right)\left(2\cos(\delta_i-\phi)\sin(\delta_i-\phi)\right)\right], \tag{31}$$

$$\frac{\partial J}{\partial\phi} = -2k^2\sum_{i=1}^{M}\left[\left(\mathbf{r}_i\cdot\frac{\partial\mathbf{u}}{\partial\phi}\right)^2\left(\cos(\delta_i-\phi)\sin(\delta_i-\phi)\right)+\left(\mathbf{r}_i\cdot\frac{\partial\mathbf{u}}{\partial\phi}\right)\left(\mathbf{r}_i\cdot\frac{\partial^2\mathbf{u}}{\partial\phi^2}\right)\left(1+\cos^2(\delta_i-\phi)\right)\right]$$
$$-2\sum_{i=1}^{M}\cos(\delta_i-\phi)\sin(\delta_i-\phi). \tag{32}$$

Based on Eq. (16) it is seen that for a given DOA with a given geometry and number of sensors, the bias in the source DOA estimate can be controlled by changing the sensor orientation angles $\boldsymbol{\delta}$. For biased estimators, minimizing the mean square

Table 2
Two configurations of a U-AVS ULA with an arbitrary orientation.

	U-AVS ULA with an arbitrary configuration
Configuration 1	$\boldsymbol{\delta} = [10°, 118°, 75°, 49°, 138°, 85°, 107°, 25°, 144°, 37°]$
Configuration 2	$\boldsymbol{\delta} = [70°, 75°, 80°, 85°, 90°, 95°, 100°, 105°, 110°, 115°]$

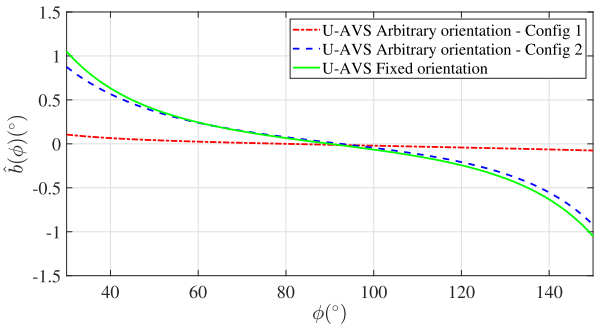

Fig. 5. Variation of the bias in the source DOA estimates based on a U-AVS ULA for all the three configurations of a U-AVS ULA.

error (MSE) of the estimate ($\widehat{\phi}$) becomes the optimal criterion based upon which the DOA performance is evaluated and it can be written as:

$$\mathrm{MSE}(\phi) = \mathbb{E}\left\{ \left\| \widehat{\phi} - \phi \right\|^2 \right\} \approx \left(\widehat{b}(\phi) \right)^2 + \mathrm{CRB_b}(\phi). \tag{33}$$

Considering the expressions in Eqs. (14), (26) and (33), three contrasting configurations of a U-AVS ULA are considered for the purpose of illustration. It includes one with a fixed orientation ($\delta = 90°$) and two with an arbitrary orientations $\boldsymbol{\delta}$, as listed in Table 2. In the first configuration, all the sensors are oriented randomly whereas in the second configuration, the sensor orientation angles are in the region between 70° and 115°.

The bias in the source DOA estimate of a U-AVS array and the MSE of all the sensor configurations with respect to ϕ are respectively plotted in Figs. 5 and 7. Also the derivative of bias with respect to ϕ is plotted in Fig. 6 for all the three configurations of the U-AVS ULA. All the plots in Figs. 5–7 are considered for a ϕ between 30° and 150°, as the bias expression approximations in eq. (16) are reasonably valid for this range as seen in Fig. 3.

It can be observed from Fig. 5, that the bias in the DOA estimate for all ϕ is small for the first configuration of the U-AVS ULA. For the U-AVS ULA with a fixed orientation ($\delta = 90°$) and for the second configuration of a U-AVS ULA with an arbitrary orientation, the bias is small in the region where the sensors are aimed at and increases as ϕ diverges from this region.

In Fig. 6, we observe that the rate of change of bias with respect to ϕ is negative for all three configurations, due to which the biased CRB of a U-AVS ULA is lower than that of the corresponding unbiased CRB. Especially for the fixed orientation configuration and for the second configuration of a U-AVS ULA, the change in bias $\left(\frac{\partial \widehat{b}(\phi)}{\partial \phi} \right)$ rapidly grows as ϕ differs from the region the sensors point at, yielding a lower biased CRB than the corresponding unbiased version.

The MSE of all the sensor configurations is shown in Fig. 7. For an APS and an AVS ULA, the MSE is the same as the CRB, since they result in an asymptotically unbiased estimate of the source DOA. On the other hand, for a U-AVS ULA, the MSE is comprised of the bias, the change in bias and the CRB as seen in Eq. (33). For the fixed orientation and the second configuration of a U-AVS

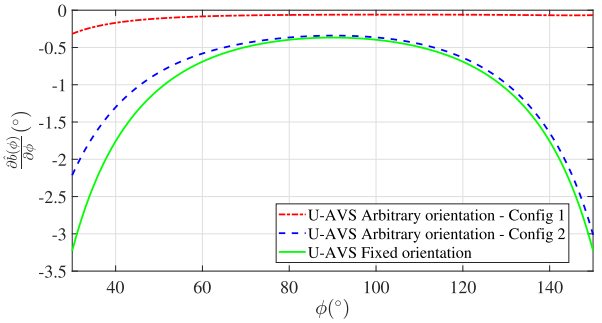

Fig. 6. Variation of the derivative of the bias in the source DOA estimates with respect to ϕ for all the three configurations of a U-AVS ULA.

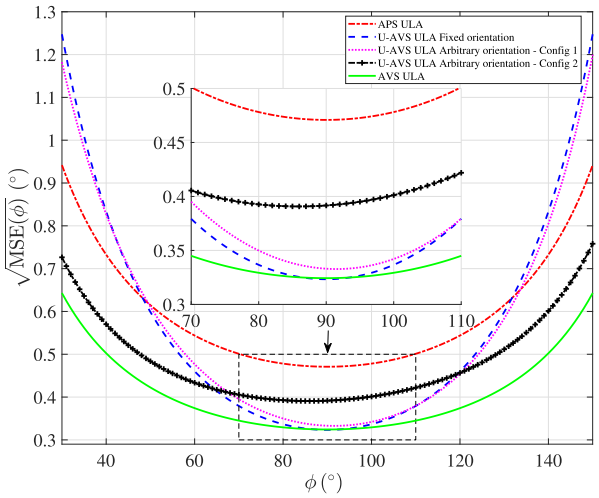

Fig. 7. Plot of ($\sqrt{\text{MSE}}$) (in °) with $M = 10, N = 10$, SNR $= 0$ dB for an APS ULA, AVS ULA and U-AVS ULA with respect to a change in ϕ.

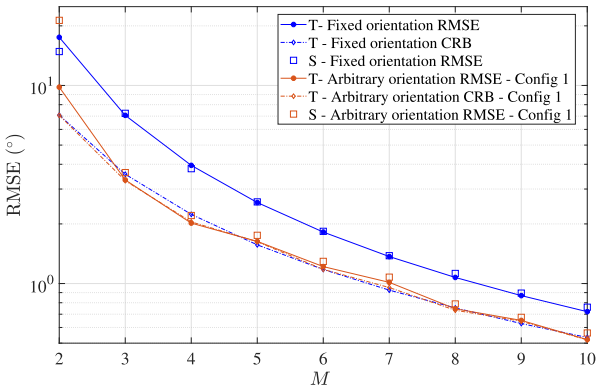

Fig. 8. Validation of the MSE expressions of a U-AVS ULA with fixed and arbitrary orientations using 1000 Monte Carlo simulations with increasing number of sensors. For the simulations we consider $N = 10$, SNR $= 0$ dB, $\phi = 45°$. Also the unbiased CRB is plotted for both fixed and arbitrary orientations. The plots of the MSE and the unbiased CRB expressions are labeled as **T** and the simulation RMSEs are labeled as **S**.

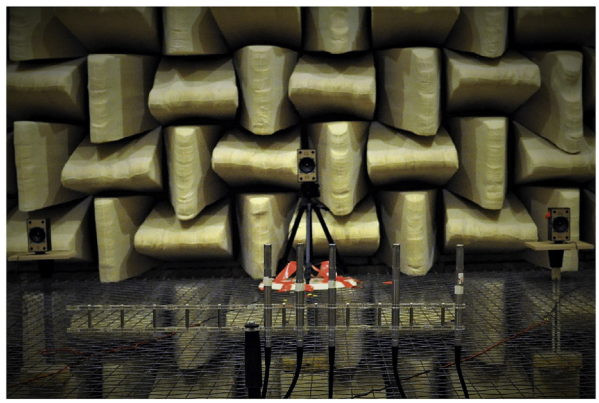

Fig. 9. Picture of the arrangement of five AVSs and three speakers, which are located on the circumference of a circle with radius $r = 360$ cm.

ULA, the MSE is similar to the results obtained for an AVS ULA for ϕ around 90° and it drifts away rapidly as ϕ differs from 90°. For the first configuration of a U-AVS ULA, the MSE lies in between the MSE of an APS and an AVS array for all ϕ. Based on the observations from Fig. 7, for a given number of sensors/aperture, it can be inferred that the MSE of the U-AVS array can be

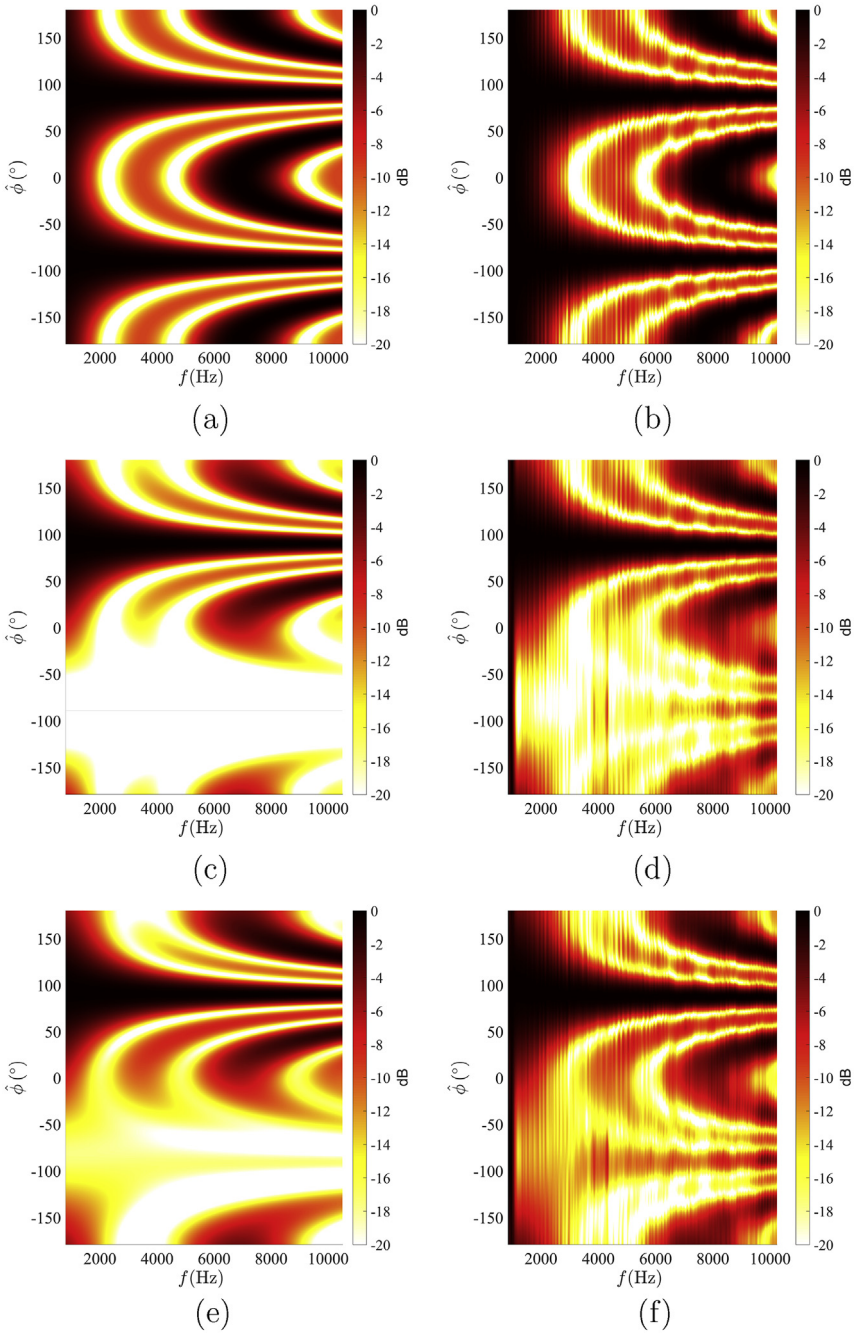

Fig. 10. Variation in the beampattern of APS (in (a), (b)), AVS (in (c), (d)) and U-AVS (in (e), (f)) ULA as the frequency of the source signal is increased with $M = 3, d = 5\,\text{cm}$ ($f_d = 3433\,\text{Hz}$) and $\phi = 90°$. The orientation angles of the U-AVS ULA are chosen as $\boldsymbol{\delta} = [57°, 124°, 109°]$. Subfigures (a), (c), (e) corresponds to simulation results and (b), (d), (f) correspond to experimental results.

modulated over the ϕ range by choosing the orientation angles of the U-AVSs appropriately.

In order to validate the MSE variation, Monte Carlo simulations with 1000 iterations were performed using the classical beamformer, as it is asymptotically optimal for a single source. The simulations were considered for the U-AVS ULA with a fixed and arbitrary orientation (Configuration 1, as listed in Table 2). The results are seen in Fig. 8. It can be observed that the simulations are in agreement with the MSE expressions derived in Eq. (33). The CRB curves for both configurations are also plotted in dashed lines for reference. It can be seen that for the fixed orientation scenario, the MSE is far greater than the equivalent CRB, as the bias in the DOA estimates is dominant. On the other hand, the MSE for a low number of sensors is not matching the theoretical MSE plots, as the bias expression based on first order approximations is not so accurate.

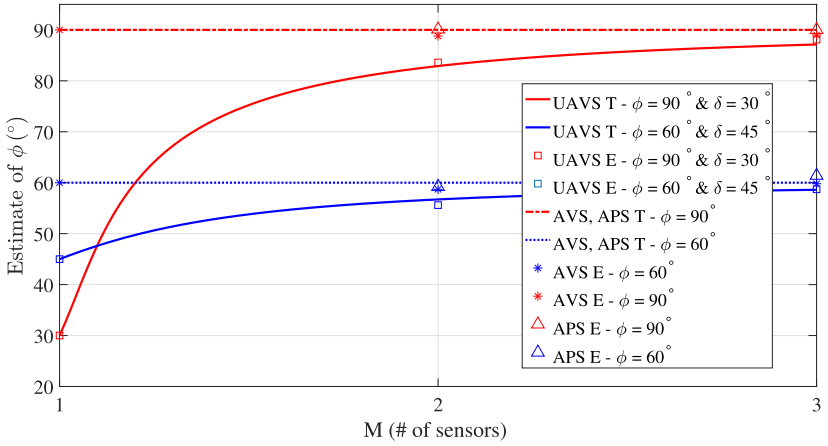

Fig. 11. Comparison of biased estimates obtained from the measurement data (labeled **E**) with the theoretical biased estimates (labeled **T**) for two scenarios with different angle of arrival (ϕ) and U-AVS sensor orientation (δ) for $M = 2, 3$. Also the DOA estimates for the equivalent AVS and APS ULA are plotted for reference.

Finally, we can conclude that for a given number of U-AVSs, application requirements such as a defined region-of-interest and geometry of the array, minimizing the MSE/function of the MSE of the DOA estimate can be chosen as a criterion to find the optimum orientation angle for each of the U-AVSs in the array such that an acceptable performance can be obtained. The related combinatorial optimization problem can be written as:

$$\arg\min_{\boldsymbol{\delta}} \quad f(\mathcal{R}), \tag{34}$$

where $f : \mathcal{M} \mapsto \mathbb{R}$ is a continuous function, defined over a manifold $\mathcal{M}$ and $\mathcal{R}$ represents a discrete angular support set, i.e., $\mathcal{R} = \{\boldsymbol{\phi}_i : \boldsymbol{\phi}_i \in \mathcal{M}, \forall 1 \leq i \leq J\}$. A simple sub-optimal choice of f can be the mean of the MSE for all $\boldsymbol{\phi}$ within $\mathcal{R}$, i.e., $\sum_{i=1}^{J} \text{MSE}(\boldsymbol{\phi}_i, \boldsymbol{\delta})$. However, the MSE expression Eq. (33) is non-convex with respect to the orientation angles, $\boldsymbol{\delta}$, which makes the optimization problem tough to solve in real-time. A sub-optimal solution can be found by using non-convex algorithms like simulated annealing or genetic algorithms or by using a convex relaxation of the MSE expression Eq. (33). Further details on this aspect are out of scope of this work as here we are mainly focusing on establishing the foundations of the U-AVS based arrays.

6. Experimental results

An experimental study was conducted in order to support the discussion and analytical expressions proposed for the U-AVS array. Firstly, the beampatterns of the APS, AVS and U-AVS ULA under a changing source signal frequency are assessed. Next, the bias in the source location estimate is compared to the theoretical value of the U-AVS ULA. A picture of the experimental setup is shown in Fig. 9, where five AVSs and three loudspeakers are seen.

The measurements were performed with the first three AVSs arranged in a ULA configuration in a fully anechoic chamber using a white Gaussian excitation, radiated by a 3 inch loudspeaker, under high SNR conditions (approximately 40 dB). For the measurements, an acquisition device with a sampling frequency of 25 kHz was used. The product specifications of the AVSs used for the experiments can be found in Ref. [34]. The inter-sensor spacing d was chosen to be 5 cm and the speaker was located at a distance of 360 cm with respect to the reference of the ULA (i.e., the range of the sources is more than 20 times the aperture of the array allowing for the far-field assumption). Although the loudspeaker was driven by white Gaussian noise, the AVS ULA was designed for a frequency of $f_d = 3433$ Hz (wavelength of $\lambda_d = 10$ cm). The pressure and particle velocity information (i.e., in $\mathbf{y}(t)$) at a given frequency are obtained by a short time discrete Fourier transform (STFT). For the STFT, a segment of 1024 samples was considered with 50% overlap. A Hanning window was applied to the data segment prior to the STFT. The measurements were performed using AVSs and the U-AVS data is obtained from the corresponding AVS data, by linearly combining each vector component data along the orientation angle in an appropriate way.

6.1. Beampattern variation due to changes in the source signal frequency

The beampattern variation of an APS, AVS and U-AVS ULA with respect to changes in the frequency is computed numerically considering the experimental sensor arrangement described above along with Eq. (5) The results are shown in Fig. 10 (a), (c) and (e). The orientation angles ($\boldsymbol{\delta}$) of the U-AVS ULA are chosen randomly between 50° and 130°. It can be noted from Fig. 10 (a), (c) and (e) that the AVS and U-AVS ULA beampattern, in comparison to the equivalent aperture APS ULA, preserve the VGM modulation based directivity even at low frequencies. Furthermore, the left/right ambiguity lobe is suppressed for both the AVS and

U-AVS ULA beampattern.

In Fig. 10 (b), (d) and (f), the equivalent beampattern of an APS, AVS and U-AVS ULA are plotted based on the measurement data. As it can be seen, the experimental results are comparable with the theoretical ones presented in Fig. 10 (a), (c) and (e). The discrepancies between the experimental and the numerical results can be explained due to the unequal source radiation, as well as small positioning and calibration errors.

6.2. Bias variation due to an increase in the aperture of the U-AVS ULA

We compare the estimates based on the measurement data with the theoretical estimates in Fig. 11 for two scenarios ($\phi = 60°, \delta = 45°$ and $\phi = 90°, \delta = 30°$). As shown, the estimates based on the measurement data are very similar to the theoretical estimates of the source location. Furthermore, we observe that the bias in the estimates based on the measurement data reduces as the aperture of the ULA increases. The DOA estimates based on the equivalent AVS and APS ULA measurement data are also indicated in Fig. 11 for reference. The small mismatches between the theoretical and the experimental data are probably due to the positioning and orientation errors during the test.

7. Conclusions

In this paper, a new configuration of the AVS with two transducers (one pressure and one particle velocity transducer) is introduced, which is referred to as the U-AVS (Uniaxial Acoustic Vector Sensor). Adopting the matched filter based beampatterns, the behavior of a U-AVS array is explored. Similar to an AVS array, it is shown that the beampattern of a U-AVS array with a fixed orientation can be decomposed as the product of an equivalent APS array beampattern and a VGM term. Based on this decomposition, the advantages of an AVS array are preserved to a considerable extent in the case of a U-AVS array. In order to observe this aspect, a numerical and experimental study was performed to validate the variation of the beampattern of an APS, AVS and U-AVS ULA with respect to a change in the source signal frequency. It is found that the DOA estimates based on the classical beamforming approach for a U-AVS array result in biased estimates. Based on the first order Taylor expansion of the beamforming function, the bias in the estimate is quantified and also validated by performing numerical simulations and experiments. Further, the bias approximation accuracy is numerically studied with a varying number of sensors and ROIs. It is seen that the bias can be altered by changing the orientation angles of the U-AVSs in an array with a fixed aperture.

The CRB for a single source scenario is evaluated for a U-AVS array and compared with the APS and AVS array. Further, the expressions for the biased CRB and the MSE of a U-AVS array were derived and their behavior was studied for three specifically chosen ULA configurations. Based on the numerical analysis of those three ULA configurations we can observe that the MSE of the estimates over different DOAs can be modulated by changing the orientations of the U-AVSs in the array. Also the MSE is numerically validated for an increasing number of sensors.

The numerical and experimental validation of the proposed theoretical framework verifies that the analytical expressions derived can be used to quantify the estimation error for a given geometry and they can ultimately be adopted to optimize the orientations of the U-AVSs for a set of requirements.

Acknowledgements

This work is part of the ASPIRE project (project 14926 within the STW OTP programme), which is financed by the Netherlands Organization for Scientific Research (NWO).

Appendix A. Bias expression for U-AVS array

Here, we derive the bias expression of Eq. (16) in Section 4. By taking the first and second order derivatives of $f(\phi)$ with respect to ϕ, we obtain (for brevity the dependence on $\boldsymbol{\delta}$ is dropped from the steering vectors and its derivatives)

$$\widehat{b}(\phi) = -\frac{\mathbf{d}^H(\phi)\mathbf{R}_\mathbf{y}\mathbf{a}(\phi) + \mathbf{a}^H(\phi)\mathbf{R}_\mathbf{y}\mathbf{d}(\phi)}{\dot{\mathbf{d}}^H(\phi)\mathbf{R}_\mathbf{y}\mathbf{a}(\phi) + 2\mathbf{d}^H(\phi)\mathbf{R}_\mathbf{y}\mathbf{d}(\phi) + \mathbf{a}^H(\phi)\mathbf{R}_\mathbf{y}\dot{\mathbf{d}}(\phi)}, \tag{A.1}$$

where $\dot{\mathbf{d}}(\phi) = \frac{\partial^2 \mathbf{a}(\phi)}{\partial \phi^2}$. We consider here a random source signal $s(t)$ with zero mean and variance σ_s^2, and additive noise with zero mean and variance σ_n^2. For this configuration $\mathbf{R}_\mathbf{y} = \sigma_\mathrm{s}^2\mathbf{a}(\phi)\mathbf{a}^H(\phi) + \sigma_\mathrm{n}^2\mathbf{I}$. After evaluating $\mathbf{d}(\phi)$ and $\dot{\mathbf{d}}(\phi)$, the following inner products can be derived:

$$\mathbf{a}^H(\phi)\mathbf{a}(\phi) = \underbrace{M + \sum_{i=1}^{M} \cos^2(\delta_i - \phi)}_{R}, \tag{A.2}$$

$$\mathbf{d}^H(\phi)\mathbf{a}(\phi) = -\mathrm{j}\quad \underbrace{k\sum_{i=1}^{M}\left(\mathbf{r}_i\cdot\frac{\partial\mathbf{u}}{\partial\phi}\right)\left(1+\cos^2(\delta_i-\phi)\right)}_{L} + \underbrace{\sum_{i=1}^{M}\cos(\delta_i-\phi)\,\sin(\delta_i-\phi)}_{S}, \tag{A.3}$$

$$\mathbf{d}^H(\phi)\mathbf{d}(\phi) = \underbrace{k^2\sum_{i=1}^{M}\left(\mathbf{r}_i\cdot\frac{\partial\mathbf{u}}{\partial\phi}\right)^2\left(1+\cos^2(\delta_i-\phi)\right)+\sum_{i=1}^{M}\sin^2(\delta_i-\phi)}_{W}. \tag{A.4}$$

$$\begin{aligned}\dot{\mathbf{d}}^H(\phi)\mathbf{a}(\phi) = {}& \mathrm{j}k\sum_{i=1}^{M}\left(\mathbf{r}_i\cdot\frac{\partial^2\mathbf{u}}{\partial\phi^2}\right)\left(1+\cos^2(\delta_i-\phi)\right)+2\mathrm{j}k\sum_{i=1}^{M}\left(\mathbf{r}_i\cdot\frac{\partial\mathbf{u}}{\partial\phi}\right)\cos(\delta_i-\phi)\,\sin(\delta_i-\phi)\\ &\underbrace{-k^2\sum_{i=1}^{M}\left(\mathbf{r}_i\cdot\frac{\partial\mathbf{u}}{\partial\phi}\right)^2\left(1+\cos^2(\delta_i-\phi)\right)-\sum_{i=1}^{M}\cos^2(\delta_i-\phi)}_{J}.\end{aligned} \tag{A.5}$$

Substituting Eqs. (A.2)– (A.5) into Eq. (A.1), finally leads to Eq. (16).

Appendix B. CRB expression for a U-AVS array and a single source

The CRB expression for a U-AVS array is considered in this section and the same steps can be followed to derive the expressions for an equivalent AVS and APS array. The inner products $\mathbf{a}^H(\phi)\mathbf{a}(\phi)$, $\mathbf{d}^H(\phi)\mathbf{a}(\phi)$ and $\mathbf{d}^H(\phi)\mathbf{d}(\phi)$ required for the evaluation of the CRB expression are already captured in Eqs. (A.2)–(A.4), respectively. Based on the inner product results, we now evaluate $\mathbf{d}^H\mathbf{a}\mathbf{a}^H\mathbf{d}$, $\mathbf{d}^H\mathbf{d}\mathbf{a}^H\mathbf{a}$ and subsequently $\mathbf{d}^H\mathbf{\Pi}_c\mathbf{d}$ specified in Eq. (18) (for brevity the dependence on ϕ is dropped):

$$\begin{aligned}\mathbf{d}^H\mathbf{a}\mathbf{a}^H\mathbf{d} = {}& k^2\sum_{i=1}^{M}\sum_{j=1}^{M}\left(\mathbf{r}_i\cdot\frac{\partial\mathbf{u}}{\partial\phi}\right)\left(\mathbf{r}_j\cdot\frac{\partial\mathbf{u}}{\partial\phi}\right)\left(1+\cos^2(\delta_i-\phi)\right)\left(1+\cos^2(\delta_j-\phi)\right)\\ &+\sum_{i=1}^{M}\sum_{j=1}^{M}\sin(\delta_i-\phi)\,\cos(\delta_i-\phi)\sin(\delta_j-\phi)\,\cos(\delta_j-\phi),\end{aligned} \tag{B.1}$$

$$\begin{aligned}\mathbf{d}^H\mathbf{d}\mathbf{a}^H\mathbf{a} = {}& Mk^2\sum_{i=1}^{M}\left(\mathbf{r}_i\cdot\frac{\partial\mathbf{u}}{\partial\phi}\right)^2(1+\cos^2(\delta_i-\phi))+M\sum_{i=1}^{M}\sin^2(\delta_i-\phi)\\ &+k^2\sum_{i=1}^{M}\sum_{j=1}^{M}\left(\mathbf{r}_i\cdot\frac{\partial\mathbf{u}}{\partial\phi}\right)^2\cos^2(\delta_j-\phi)\left(1+\cos^2(\delta_i-\phi)\right)+\sum_{i=1}^{M}\sum_{j=1}^{M}\cos^2(\delta_j-\phi)\sin^2(\delta_i-\phi),\end{aligned} \tag{B.2}$$

$$\begin{aligned}\mathbf{d}^H\mathbf{\Pi}_c\mathbf{d} &= \frac{\mathbf{d}^H\mathbf{d}\mathbf{a}^H\mathbf{a}-\mathbf{d}^H\mathbf{a}\mathbf{a}^H\mathbf{d}}{\mathbf{a}^H\mathbf{a}},\\ &= \frac{P_G}{M+\sum_{i=1}^{M}\cos^2(\delta_i-\phi)},\end{aligned} \tag{B.3}$$

with P_G given in Eq. (24). Further, the $\mathbf{U}$ term specified in Eq. (18) results in the scalar U:

$$U = \frac{\left(M+\sum_{i=1}^{M}\cos^2(\delta_i-\phi)\right)\sigma_s^4}{\left(M+\sum_{i=1}^{M}\cos^2(\delta_i-\phi)\right)\sigma_s^2+\sigma_n^2}. \tag{B.4}$$

Finally, the CRB expression of Eq. (18) reduces to:

$$\mathrm{CRB}(\phi) = \frac{1}{2NP_G}\left(\frac{\left(M+\sum_{i=1}^{M}\cos^2(\delta_i-\phi)\right)}{\mathrm{SNR}}+\frac{1}{(\mathrm{SNR})^2}\right). \tag{B.5}$$

Appendix C. Supplementary data

Supplementary data related to this article can be found at https://doi.org/10.1016/j.jsv.2018.08.031.

References

[1] H.L. Van, Trees, Optimum Array Processing. Part {IV} of Detection, Estimation, and Modulation Theory, Wiley-Interscience, New York, 2002.
[2] R. Schmidt, Multiple emitter location and signal parameter estimation, IEEE Trans. Antenn. Propag. 34 (3) (1986) 276–280.
[3] I.N. El-Behery, R.H. MacPhie, Maximum-likelihood estimation of source parameters from time-sampled outputs of a linear array, J. Acoust. Soc. Am. 62 (1) (1977) 125–134.
[4] P. Stoica, A. Nehorai, MUSIC, maximum likelihood, and Cramer-Rao bound, IEEE Trans. Acoust. Speech Signal Process. 37 (5) (1989) 720–741.
[5] P. Stoica, A. Nehorai, MUSIC, maximum likelihood, and Cramér-Rao bound: further results and comparisons, IEEE Trans. Acoust. Speech Signal Process. 38 (12) (1990) 2140–2150.
[6] H. Krim, M. Viberg, Two decades of array signal processing research: the parametric approach, IEEE Signal Process. Mag. 13 (4) (1996) 67–94.
[7] H.-E. De Bree, The Microflown E-book, Microflown Technologies, Arnhem.
[8] M. Hawkes, A. Nehorai, Acoustic vector sensor beamforming and Capon direction estimation, IEEE Trans. Signal Process. 46 (9) (1998) 2291–2304.
[9] A. Nehorai, E. Paldi, Acoustic vector-sensor array processing, IEEE Trans. Signal Process. 42 (9) (1994) 2481–2491.
[10] W.-Q. Jing, D.F. Comesaña, D.P. Cabo, Sound source localisation using a single acoustic vector sensor and multichannel microphone phased arrays, INTER-NOISE and NOISE-CON Congress and Conference Proceedings, vol. 249, 2014.
[11] D. Levin, E.A.P. Habets, S. Gannot, Maximum likelihood estimation of direction of arrival using an acoustic vector-sensor, J. Acoust. Soc. Am. 131 (2) (2012) 1240–1248.
[12] Z. Liu, X. Ruan, J. He, Efficient 2-D DOA estimation for coherent sources with a sparse acoustic vector-sensor array, Multidimens. Syst. Signal Process. 24 (1) (2013) 105–120.
[13] M.K. Awad, K.T. Wong, Recursive least-squares source tracking using one acoustic vector sensor, IEEE Trans. Aero. Electron. Syst. 48 (4) (2012) 3073–3083.
[14] X. Zhong, A.B. Premkumar, Particle filtering approaches for multiple acoustic source detection and 2-D direction of arrival estimation using a single acoustic vector sensor, IEEE Trans. Signal Process. 60 (9) (2012) 4719–4733.
[15] M. Shujau, C.H. Ritz, I.S. Burnett, Using in-air acoustic vector sensors for tracking moving speakers, in: Signal Processing and Communication Systems (ICSPCS), 2010 4th International Conference on, IEEE, 2010, pp. 1–5.
[16] M. Hawkes, A. Nehorai, Bearing estimation with acoustic vector-sensor arrays, in: AIP Conference Proceedings, 1996, pp. 345–358.
[17] D. Y. Levin, E. A. P. Habets, S. Gannot, Near-field Signal Acquisition for Smart Glasses Using Two Acoustic Vector-sensors, arXiv:1602.06582.
[18] J.P. Kitchens, Acoustic Vector-sensor Array Performance, Master's thesis, Massachusetts Institute of Technology, 2008.
[19] J.P. Kitchens, Acoustic Vector-sensor Array Processing, Ph.D. thesis, 2010. DTIC Document.
[20] M. Hawkes, A. Nehorai, Effects of sensor placement on acoustic vector-sensor array performance, IEEE J. Ocean. Eng. 24 (1) (1999) 33–40.
[21] Y. Wu, Z. Hu, H. Luo, Y. Hu, Source number detectability by an acoustic vector sensor linear array and performance analysis, Ocean. Eng., IEEE J. 39 (4) (2014) 769–778.
[22] M. Hawkes, A. Nehorai, Acoustic vector-sensor processing in the presence of a reflecting boundary, IEEE Trans. Signal Process. 48 (11) (2000) 2981–2993.
[23] M. Hawkes, A. Nehorai, Acoustic vector sensor correlations in ambient noise, IEEE J. Ocean. Eng. 26 (3) (2001) 337–347.
[24] D. Levin, S. Gannot, E.A.P. Habets, Direction-of-arrival estimation using acoustic vector sensors in the presence of noise, in: 2011 IEEE International Conference on Acoustics, Speech and Signal Processing (ICASSP), IEEE, 2011, pp. 105–108.
[25] Y. Song, Y.L. Li, K.T. Wong, Acoustic direction finding using a pressure sensor and a uniaxial particle velocity sensor, IEEE Trans. Aero. Electron. Syst. 51 (4) (2015) 2560–2569.
[26] Y. Song, K.T. Wong, Azimuth-elevation direction finding using a microphone and three orthogonal velocity sensors as a non-collocated subarray, J. Acoust. Soc. Am. 133 (4) (2013) 1987–1995.
[27] Y. Song, K.T. Wong, Acoustic direction finding using a spatially spread tri-axial velocity sensor, IEEE Trans. Aero. Electron. Syst. 51 (2) (2015) 834–842.
[28] C.H. Lee, H.R.L. Lee, K.T. Wong, M. Razo, The spatial-matched-filter beampattern of a biaxial non-orthogonal velocity sensor, J. Sound Vib. 367 (2016) 250–255.
[29] K.T. Wong, M.D. Zoltowski, Root-MUSIC-based azimuth-elevation angle-of-arrival estimation with uniformly spaced but arbitrarily oriented velocity hydrophones, IEEE Trans. Signal Process. 47 (12) (1999) 3250–3260.
[30] Y. Song, K.T. Wong, Y. Li, Direction finding using a biaxial particle-velocity sensor, J. Sound Vib. 340 (2015) 354–367.
[31] K.N. Ramamohan, Acoustic Vector Sensor Based Source Localization, Master's Thesis, Delft University of Technology, 2016.
[32] A. Nehorai, E. Paldi, Vector-sensor array processing for electromagnetic source localization, IEEE Trans. Signal Process. 42 (2) (1994) 376–398.
[33] S. Kay, Y.C. Eldar, Rethinking biased estimation, IEEE Signal Process. Mag. 25 (3) (2008) 133.
[34] Microflown, USP Regular Product Datasheet, Microflown Technologies, 2018, http://microflown.com/products/standard-probes/usp-regular.html.